Molecular basis of ligand recognition and activation of succinate receptor

Changyao Li[1,2,3,7], Heng Liu[1,7], Jingru Li[4,7], Haoran Zhu[5], Wei Fu[5*], H. Eric Xu[1,3,5,6,8*]

[1] The CAS Key Laboratory of Receptor Research, Shanghai Institute of Materia Medica, Chinese Academy of Sciences, Shanghai 201203, China

[2] Lingang Laboratory, Shanghai 200031, China

[3] School of Life Science and Technology, ShanghaiTech University, Shanghai 201210, China

[4]School of Chinese Materia Medica, Nanjing University of Chinese Medicine, Nanjing 210023, China

[5]School of Pharmacy, Fudan University, Shanghai, 201301, PR China

[6]University of Chinese Academy of Sciences, Beijing 100049, China

[7]These authors contributed equally

[8]Lead Contact

*Correspondence: wfu@fudan.edu.cn (Fu Wei), eric.xu@simm.ac.cn (H.E.X)

Abstract

Succinic acid, a tricarboxylic acid (TCA) cycle intermediate, significantly influences mitochondrial reactive oxygen species homeostasis through the G protein-coupled succinate receptor (SUCR1, also called GPR91), linking it to various physiological and pathological processes. Despite SUCR1's pivotal role in mediating effects leading to liver fibrosis, hypertension, angiogenesis, inflammation, and offering a therapeutic target for multiple diseases, its activation mechanism by diverse ligands and interaction with downwards G protein remains poorly understood. This study presents the cryo-electron microscopy (cryo-EM) structures of SUCR1 in complex with inhibitory G protein (G_i) bound to succinic acid, maleic acid, and compound 31, a high-affinity agonist. These structures elucidate the distinct ligand binding modes, uncover the activation signal cascade, and detail the G protein coupling mechanism of SUCR1. Our findings provide a comprehensive structural basis for SUCR1 activation, paving the way for structure-based drug design aimed at SUCR1-related pathologies.

Dear Editor,

Succinic acid, once considered merely a tricarboxylic acid (TCA) cycle intermediate[1], has been recognized for its significant role in influencing mitochondrial reactive oxygen species (ROS) homeostasis[2]. This is largely mediated through the G protein-coupled succinate receptor (SUCR1, also known as GPR91), which has emerged as a vital link connecting metabolic status to a myriad of physiological and pathological processes. SUCR1 is intricately involved in the regulation of blood pressure[3], angiogenesis[4], inflammation[5], and has been implicated in the pathogenesis of liver fibrosis[6], hypertension, and rheumatic arthritis[6]. These multifaceted roles highlight the receptor's potential as a promising therapeutic target for a wide spectrum of diseases. However, the molecular underpinnings of SUCR1's activation by various ligands and its subsequent interaction with the inhibitory G protein (G_i) have remained elusive, obscuring our understanding of its broad physiological significance and therapeutic potential.

To address this knowledge gap, we determined three cryo-electron microscopy(cryo-EM) structures of the human SUCR1-G_i complexes with the endogenous succinic acid, maleic acid, and the structurally related compound 31, a higher affinity agonist, using combinatorial approaches of BRIL fusion, G_i engineering, and stabilising antibody scFv16, which had previously been used successfully in solving several GPCR/G-protein complexes[7,8] (Supplementary information, Fig. S1). Succinic acid, maleic acid, and compound 31 bound SUCR1-G_i complexes were solved at global resolutions of 2.75 Å, 2.69 Å, and 2.48 Å, respectively (Fig. 1a; Supplementary information, Figs. S2-S4 and Table S1).

In all structures, SUCR1 adopts an active-like state typical of GPCR-G protein coupling. The overall structure of SUCR1 is similar to that of the medium-chain fatty acid receptor, GPR84 (PDB: 8J18)[9] with root mean square deviation (RMSD) of 0.36 Å for the Cα

atoms of SUCR1 (residues 10-309) and GPR84 (residues 8-395). In both receptors, their ECL2 forms the lid of the ligand-binding pocket (Fig. 1b). Due to the smaller ligands and more compact ligand-binding pockets, the structure of SUCR1 is leaner compared to other class A GPCR including GPR84, with the extracellular domains of TM1, TM5, and TM6 shifting inward to the ligand binding pocket (Fig. 1b). In addition, structural comparisons indicate that the TM1 of SUCR1 is significantly longer than GPR84, which may be related to the stability of its receptor (Fig. 1b).

In the structure of the succinic acid-SUCR1 complex, succinic acid is securely held within a binding pocket formed by TM1, TM2, TM3, TM7, and ECL2, which exhibits a shape resembling the letter "C". The pocket is highly electrostatically positive to accommodate the negative succinic acid. The two carboxylic acids of succinic acid are directed towards the extracellular side of the ligand binding pocket (Supplementary information, Fig. S5a), and form hydrogen bonds with $Y30^{1.39}$ and $Y83^{2.64}$ and from ionic bonds with $R99^{3.29}$ and $R281^{7.39}$, respectively (Fig. 1c). In addition, $Y30^{1.39}$ also forms hydrogen bond and $R281^{7.39}$, stabilizing the hydrophilic environment of the binding pocket (Fig. 1c). As mentioned above, ECL2 is located on the top of the succinic acid and covers the entry of the ligand-binding pocket. The main chain amine in $F175^{ECL2}$ forms a hydrogen bond with the carboxylic acid of succinic acid (Supplementary information, Fig. S5a). Simultaneously, the alkyl portion in the middle of the ligand predominantly orients itself towards the bottom of the ligand binding pocket, interacting with hydrophobic residues, including $L79^{2.60}$, $L102^{3.32}$, and $F285^{7.43}$, to establish hydrophobic interactions (Fig. 1c).

Maleic acid is the analogue of succinic acid, with an alkene in the alkyl portion. The maleic acid is almost aligning with succinic acid in the bonding pocket of SUCR1 structure. In the maleic acid-bound SUCR1 structure, the carboxylic acids in the same side forms polar interactions with residues from SUCR1, such as $Y30^{1.39}$, $Y83^{2.64}$, $R99^{3.29}$, $H103^{3.33}$, and $R281^{7.39}$ (Fig. 1d). Maleic acid forms hydrogen bond with

D174^{ECL2} (Supplementary information, Fig. S5b). Alanine substitution at D174^{ECL2} reduces receptor activation by maleic acid, underlining ECL2's significance in SUCR1 activation by endogenous ligands (Supplementary information, Fig. S6b). In the maleic acid-SUCR1-G_i structure, the alkene of maleic acid also forms hydrophobic interactions with L79$^{2.60}$, L102$^{3.32}$, and F285$^{7.43}$ similar to succinic acid (Fig. 1d). Alanine mutations in the binding pocket, including Y30$^{1.39}$, L79$^{2.60}$, Y83$^{2.64}$, R99$^{3.29}$, and R281$^{7.39}$, significantly impaired the activation potential of succinic acid and maleic acid, underscoring their essential roles in SUCR1 function (Fig. 1e, 1f; Supplementary information, Fig. S6 and Table S2, S3). These findings further underscore the intricate molecular interactions that govern SUCR1 regulation and activation by succinic acid and maleic acid.

Compound 31 is a synthetic small molecule that activates SUCR1 with high potency[10]. In this study we found that compound 31 activated SUCR1 by G_i signaling pathway with over around 100 folds than succinic acid and maleic acid (Supplementary information, Fig. S6). The structure of compound 31 is composed of part 1 “succinic acid” motif and part 2 “two-ring” motif (Supplementary information, Fig. S7a). Comparison of the compound 31-bound SUCR1 structure with the succinic acid-bound structure reveals that the sidechain of R99$^{3.29}$ is deflected, leading to the formation of an extended pocket (Supplementary information, Fig. S7b). In ligand binding pocket of the compound 31-bound SUCR1 structure, the part 1 “succinic acid” motif of compound 31 partially aligns with the position of succinic acid or maleic acid (Supplementary information, Fig. S7b), forming polar interactions with surrounding amino acids such as Y30$^{1.39}$, Y83$^{2.64}$, and R281$^{7.39}$, and nonpolar interactions with some amino acids such as L79$^{2.60}$, L102$^{3.33}$, F285$^{7.43}$(Fig. 1g). In addition, similar to the maleic acid-SUCR1 structure, the carboxylic acid in part 1 “succinic acid” motif of compound 31 also forms hydrogen bond with D174^{ECL2} (Supplementary information, Fig. S7c). While the part 2 “two-ring” motif of compound 31 occupies the expanded pocket, the pyridine in compound 31 is limited by L79$^{2.60}$, W88^{ECL1}, N98$^{3.28}$, and R99$^{3.29}$ (Fig. 1h). In addition,

the benzene ring in compound 31 is clamped by Y83$^{2.64}$ and W88^{ECL1} (Fig. 1h). The formation of interactions with surrounding SUCR1 by the part 2 “two-ring” motif may account for the significantly stronger potency of SUCR1 receptors by compound 31 than by succinic acid and maleic acid. Mutation of Y30$^{1.39}$, L79$^{2.60}$, N87^{ECL1}, N98$^{3.28}$, R99$^{3.29}$, and R281$^{7.39}$ in SUCR1 reduced compound 31-induced signaling responses, confirming the essential roles of these residues in ligand binding and receptor activation (Fig. 1i, j; Supplementary information, Fig. S6 and Table S4). In summary, these intricate details reveal the comprehensive mechanism behind SUCR1 activation by the synthetic agonist compound 31.

Comparisons of the above three complex structures revealed that SUCR1 had similar overall structural arrangements, with RMSD values for Cα atoms of the entire receptor ranging between 0.33-0.50 Å (Fig. 1k, l). Considering the similarity of the three complexes, we chose the succinic acid-SUCR1 complex for a detailed analysis of SUCR1 activation. Comparing the active succinic acid-SUCR1 complex structure with the inactive β_2AR structure (PDB: 8JJO)[11], the cytoplasmic end of TM6 in SUCR1 displays a pronounced outward movement while the cytoplasmic part of TM7 shifts inward. This rearrangement accommodates the C-terminal α5 helix of the $G\alpha_i$ subunit, a key feature of Class A GPCR activation (Fig. 1m). In general, many GPCRs are able to sense ligand binding via a conserved toggle switch, exemplified by W$^{6.48}$ of β_2AR. At the equivalent position of the toggle switch[12], SUCR1 has F245$^{6.48}$, which does not directly contact any of the above agonists. Instead, L102$^{3.32}$ and F285$^{7.43}$ directly contact the alkyl portion (Fig. 1l), which pushes downward of F285$^{7.43}$ to pack against L106$^{3.36}$ and F245$^{6.48}$, which then leads to rotations of the P$^{5.50}$-I$^{3.40}$-F$^{6.44}$ motif. This chain of conformational changes ultimately leads to the outward bending of TM6 to accommodate G_i coupling.

In this paper, we have determined cryo-EM structures of SUCR1 in complex with succinic acid, maleic acid, and compound 31. The detailed structural analysis provided

by this study not only enhances our understanding of SUCR1-ligand interactions but also underscores the potential of structure-based drug design in developing targeted therapies for diseases associated with dysregulated succinic acid signaling, such as hypertension, inflammation, and metabolic disorders. The identification of key residues involved in ligand binding and receptor activation presents specific targets for the development of drugs aimed at modulating SUCR1 activity with high specificity and efficacy.

In conclusion, this study not only contributes to the expanding repository of GPCR structural biology but also represents a pivotal step forward in the quest for targeted therapeutics. The comprehensive structural basis for SUCR1 activation provided herein highlights the receptor's potential as a versatile and valuable target for drug design and discovery. As we continue to unravel the complex signaling networks mediated by SUCR1, the prospects for developing novel therapeutic strategies that harness the power of structure-based drug design become increasingly tangible, offering hope for the effective management and treatment of a wide range of diseases.

Acknowledgements

This work was supported by grants from CAS Strategic Priority Research Program (XDB37030103 to H.E.X.)；Shanghai Municipal Science and Technology Major Project (2019SHZDZX02 to H.E.X.); Shanghai Municipal Science and Technology Major Project (H.E.X.); The National Natural Science Foundation of China (32130022, 82121005)； the Lingang Laboratory, Grant No.LG-GG-202204-01 (H.E.X.); the National Key R&D Program of China（2022YFC2703105 to H.E.X.). The cryo-EM data were collected at the Shanghai Advanced Electron Microscope Center, Shanghai Institute of Material Medica, Chinese Academy of Sciences. We thank Q. Yuan., K. Wu., W. Hu., S. Li. and S. Zhang. for providing technical support and assistance during data collection at the Shanghai Advanced Electron Microscope Center, Shanghai Institute of Material Medica.

Author contributions

H.E.X. initiated the project. C.L. designed and screened the expression constructs of SUCR1 and prepared protein samples of succinic acid-SUCR1-G_i, maleic acid-SUCR1-G_i, and compound 31-SUCR1-G_i complexes for cryo-EM data collection, participated in cryo-EM grid inspection, and executed the functional studies. H.L. performed cryo-EM grids preparation, data acquisition, structure determination and model building, and prepared the draft of the manuscript and figures. H.Z. synthesized the compound 31 for structural study. J.L. performed cell-based function assay and participated in figure preparation. W.F. guided H.Z. to synthesize the compound 31. H.E.X. wrote the manuscript with input from all authors.

Data availability

Competing interests

The authors declare no competing interests.

REFERENCES

1 He, W. H. *et al.* Citric acid cycle intermediates as ligands for orphan G-protein-coupled receptors. *Nature* **429**, 188-193, doi:10.1038/nature02488 (2004).

2 Fonseca, M. D., Aguiar, C. J., Franco, J. A. D., Gingold, R. N. & Leite, M. F. GPR91: expanding the frontiers of Krebs cycle intermediates. *Cell Commun Signal* **14**, doi:ARTN 3 10.1186/s12964-016-0126-1 (2016).

3 Sadagopan, N. *et al.* Circulating succinate is elevated in rodent models of hypertension and metabolic disease. *Am J Hypertens* **20**, 1209-1215, doi:10.1016/j.amjhyper.2007.05.010 (2007).

4 Sapieha, P. *et al.* The succinate receptor GPR91 in neurons has a major role in retinal angiogenesis. *Nat Med* **14**, 1067-1076, doi:10.1038/nm.1873 (2008).

5 Tannahill, G. M. *et al.* Succinate is an inflammatory signal that induces IL-1β through HIF-1α. *Nature* **496**, 238-+, doi:10.1038/nature11986 (2013).

6 Li, Y. H., Woo, S. H., Choi, D. H. & Cho, E. H. Succinate causes α-SMA production through GPR91 activation in hepatic stellate cells. *Biochem Bioph Res Co* **463**, 853-858, doi:10.1016/j.bbrc.2015.06.023 (2015).

7 Maeda, S. *et al.* Development of an antibody fragment that stabilizes GPCR/G-protein complexes. *Nature Communications* **9**, doi:ARTN 3712 10.1038/s41467-018-06002-w (2018).

8 Chun, E. *et al.* Fusion Partner Toolchest for the Stabilization and Crystallization of G Protein-Coupled Receptors. *Structure* **20**, 967-976, doi:10.1016/j.str.2012.04.010 (2012).

9 Liu, H. *et al.* Structural insights into ligand recognition and activation of the medium-chain fatty acid-sensing receptor GPR84. *Nature Communications* **14**, doi:ARTN 3271 10.1038/s41467-023-38985-6 (2023).

10 Ulven, E. R. *et al.* Structure-Activity Investigations and Optimisations of Non-metabolite Agonists for the Succinate Receptor 1. *Sci Rep-Uk* **8**, doi:ARTN 10010 10.1038/s41598-018-28263-7 (2018).

11 Guo, Q. *et al.* A method for structure determination of GPCRs in various states. *Nat Chem Biol*, doi:10.1038/s41589-023-01389-0 (2023).

12 Nygaard, R., Frimurer, T. M., Holst, B., Rosenkilde, M. M. & Schwartz, T. W. Ligand binding and micro-switches in 7TM receptor structures. *Trends Pharmacol Sci* **30**, 249-259, doi:10.1016/j.tips.2009.02.006 (2009).

Figure 1

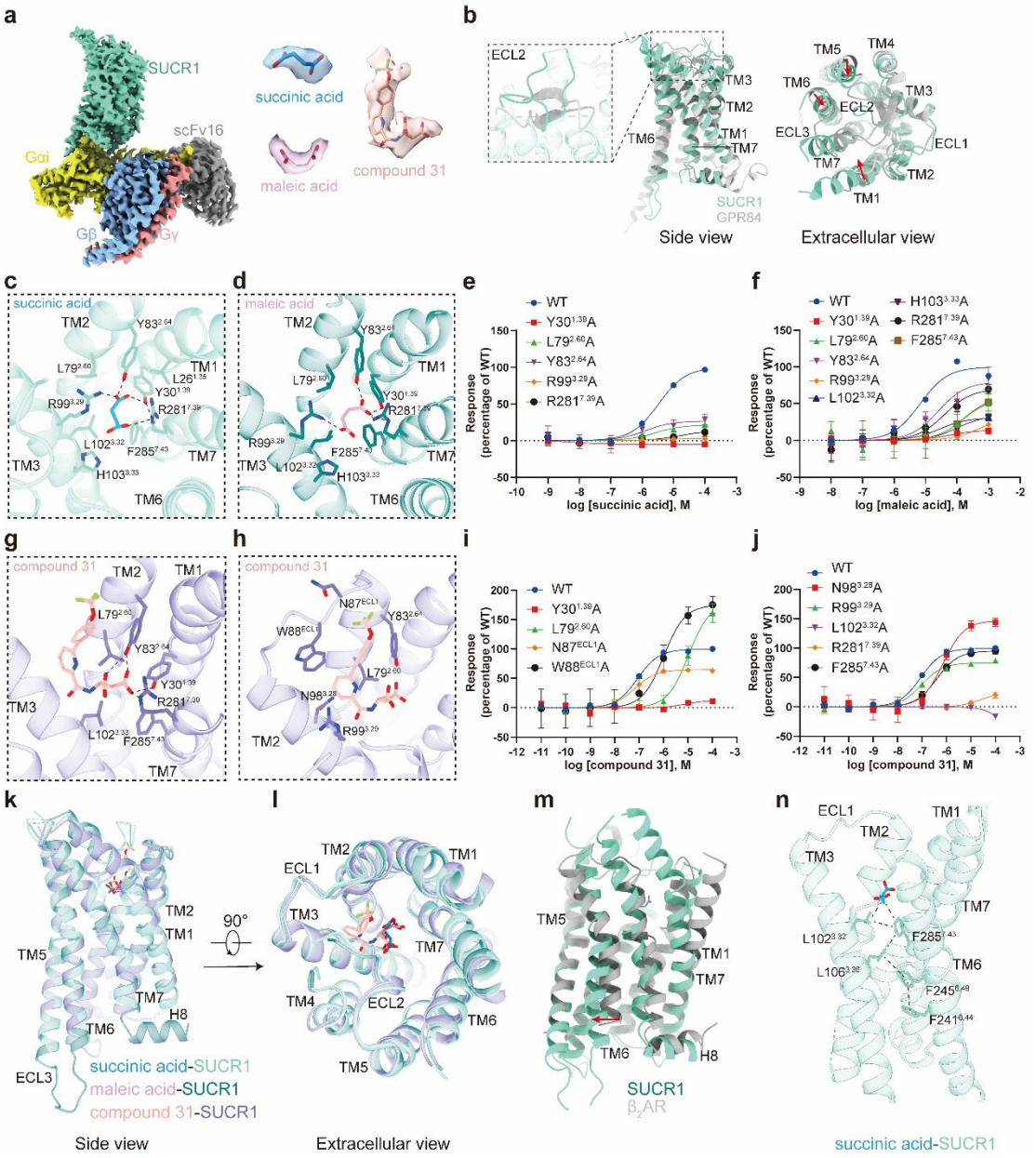

Figure 1. Cryo-EM structures of ligand recognition and activation of succinate receptor

a Cryo-EM density map and cartoon presentation of the SUCR1-G_i complex.

b Structural alignment of SUCR1 with GPR84 indicated the overall feature of SUCR1.

c, d Detailed interactions of succinic acid (**c**) and maleic acid (**d**) with residues from SUCR1.

e, f Effects of succinic acid (**e**) and maleic acid (**f**) in activating WT or mutated SUCR1.

Data are mean ± S.E.M. from 3 independent experiments (n = 3).

g, h Detailed interactions of “succinic acid” motif (**g**) and “two-ring” motif (**h**) of compound 31 with residues from SUCR1.

i, j Effects of “succinic acid” motif (**g**) and “two-ring” motif (**h**) of compound 31 in activating WT or mutated SUCR1. Data are mean ± S.E.M. from 3 independent experiments (n = 3).

k, l Side view (**k**) and extracellular view (**l**) of structural alignment of SUCR1 structures.

m Superposition of activated SUCR1 (green) with inactive β_2AR (PDB code: 8JJO). Notable conformational changes occur at intracellular ends of TM6 and TM7 upon receptor activation, side view (left) and bottom view (right).

n A hydrophobic packing among L102$^{3.32}$, L106$^{3.36}$, F241^{6,44}, F245$^{6.48}$, and F285$^{7.43}$ leads to activation of SUCR1.

Supplementary Information

Molecular basis of ligand recognition and activation of succinate receptor

Changyao Li[1,2,3,7], Heng Liu[1,7], Jingru Li[4,7], Haoran Zhu[5], Wei Fu[5*], H. Eric Xu[1,3,5,6,8*]

[1] The CAS Key Laboratory of Receptor Research, Shanghai Institute of Materia Medica, Chinese Academy of Sciences, Shanghai 201203, China

[2] Lingang Laboratory, Shanghai 200031, China

[3] School of Life Science and Technology, ShanghaiTech University, Shanghai 201210, China

[4]School of Chinese Materia Medica, Nanjing University of Chinese Medicine, Nanjing 210023, China

[5]School of Pharmacy, Fudan University, Shanghai, 201301, PR China

[6]University of Chinese Academy of Sciences, Beijing 100049, China

[7]These authors contributed equally

[8]Lead Contact

*Correspondence: wfu@fudan.edu.cn (Fu Wei), eric.xu@simm.ac.cn (H.E.X)

Materials and Methods

Methods

Cell lines

Trichoplusia ni. (High Five, Thermo Fisher) cells were grown in SIM HF Expression Medium (Sino biological, MHF1) at 27°C and 120 rpm. HEK293T cells were grown in a humidified 37°C incubator with 5% CO_2 using media supplemented with 100 I.U./mL penicillin and 100 mg/mL streptomycin (Invitrogen). The human cell lines HEK293T were maintained in DMEM (VWR) containing 10% fetal bovine serum (FBS, VWR).

Protein complex expression and purification

The wild-type human SUCR1, modified with an N-terminal thermally stabilized BRIL as a fusion protein, along with a HA signal peptide, a Flag tag and His tag epitope, was cloned into pFastBac transfer plasmid (Invitrogen). All constructs were generated using the Phanta Max Super-Fidelity DNA Polymerase (Vazyme Biotech Co.,Ltd) and verified by DNA sequencing (Genewiz). A dominant-negative (DN) $G\alpha_i$ format including mutation G203A/A326S was constructed to increase the stability of $G_{\alpha i\beta 1\gamma 2}$ complex[1]. SUCR1, $G\alpha_i$, $G_{\beta 1}$, $G_{\gamma 2}$ and scFv16 were co-expressed in *Trichoplusia ni* (Hi5) insect cells. Baculoviruses were prepared using the Bac-to-Bac Expression System (Invitrogen). Cells were infected with viruses at density of 3.0×10^6 cell/mL and cell culture was collected by centrifugation 48 h post-infection and stored at -80 degree until use.

For the purifications of succinic acid, maleic acid, and compound 31-bound SUCR1-$G\alpha_i$ complex, cell pellets were thawed in 20 mM HEPES pH 7.4, 100 mM NaCl, 5 mM $MgCl_2$, 5 mM $CaCl_2$, and protease inhibitor cocktail (TargetMol, USA). The suspensions were incubated for 1.5 h at room temperature supplemented with 50 mM/L succinic acid (TargetMol, USA), 50 mM/L maleic acid (TargetMol, USA), and 50 μM/L compound 31 and 25 mU/ml apyrase (Sigma-Aldrich), respectively. Subsequently, 0.5% (w/v) n-dodecyl-β-d-maltoside (DDM, Anatrace) and 0.1% (w/v) cholesteryl hemisuccinate (CHS, Anatrace) were added to solubilize complexes for 2.5 h at 4°C. Insoluble material was removed by centrifugation at 30,000 g for 30 min and the supernatant

was immobilized by batch binding to Nickel Sepharose resin (GE healthcare). After that, the resin was packed and washed with 20 column volumes of 20 mM HEPES pH 7.4, 100 mM NaCl, 20 mM imidazole, 0.01% (w/v) LMNG, and 0.002% (w/v) CHS, corresponding ligands with concentration that agree with above. Finally, the complex was collected in buffer containing 250 mM imidazole and concentrated using an Amicon Ultra Centrifugal Filter (MWCO 100 kDa). Complexes were loaded onto a Superdex 200 Increase 10/300 column (GE Healthcare) with buffer containing 20 mM HEPES pH 7.4, 100 mM NaCl, 0.00075% (w/v) LMNG, 0.00025% (w/v) GDN, 0.0002% (w/v) CHS, corresponding ligands with concentration that agree with above to separate complex from contaminants. Eluted fractions consisting of SUCR1-$G\alpha_i$ proteins complex were pooled and concentrated for electron microscopy experiments.

Cryo-EM grid preparation and data collection

For cryo-EM grids preparation of the SUCR1-G_i complexes, 3 μl of the protein at ~10 mg/ml were loaded onto a glow-discharged holey carbon grid (Quantifoil Au 300 mesh R1.2/1.3), and subsequently were plunge-frozen in liquid ethane using Vitrobot Mark IV (Thermo Fischer Scientific). Cryo-EM imaging was collected on a Titan Krios at 300 kV using Gatan K3 Summit detector and Falcon 4 direct electron detection device in the Cryo-Electron Microscopy Research Center, Shanghai Institute of Materia Medica, Chinese Academy of Sciences (Shanghai, China). For succinic acid and compound 31 bound SUCR1-G_i complex, cryo-EM imaging was collected on a Titan Krios at 300 kV using Gatan K3 Summit detector with a pixel size of 0.824 Å. Images were taken at a dose rate of about 8.0 e/Å2/s with a defocus ranging from -1.0 to -2.0 μm using the EPU software (FEI Eindhoven, Netherlands). The total exposure time was 8 s, and 36 frames were recorded per micrograph. For maleic acid bound SUCR1-G_i complex, cryo-EM imaging was collected on a Titan Krios equipped with a Falcon 4 direct electron detection device at 300 kV. Images were taken with a pixel size of 0.73 Å, a defocus ranging from -1.0 to -2.0 μm using the EPU software (FEI Eindhoven, Netherlands) with total dose of 50 e/Å2/s over 2.5 s exposure on each EER format movie.

Image processing and map construction

For succinic acid bound SUCR1-G_i complex, auto-picking by blob picker produced particles were subjected to interactively 2D and 3D classifications, producing 1,979,364 particles with complete complex and good quality. The selected particles were further subjected to several rounds of ab-initial reconstruction and heterogeneous refinement, resulting in a well-defined subset. Subsequent heterogeneous refinement, non-uniform refinement and local refinement generated a map with an indicated global resolution of 2.75 Å reconstructed by 573,312 particles.

For maleic acid bound SUCR1-G_i complex, auto-picking by blob picker produced particles were subjected to interactively 2D and 3D classifications, producing 1,436,056 particles with complete complex and good quality. The selected particles were further subjected to several rounds of ab-initial reconstruction and heterogeneous refinement, resulting in a well-defined subset. Subsequent heterogeneous refinement, non-uniform refinement and local refinement generated a map with an indicated global resolution of 2.69 Å reconstructed by 394,879 particles.

For compound 31-bound SUCR1-G_i complex, auto-picking by blob picker produced particles were subjected to interactively 2D and 3D classifications, producing 775,432 particles with complete complex and good quality. The selected particles were further subjected to several rounds of ab-initial reconstruction and heterogeneous refinement, resulting in a well-defined subset. Subsequent heterogeneous refinement, non-uniform refinement and local refinement generated a map with an indicated global resolution of 2.48 Å reconstructed by 385,083 particles. The overall resolution was estimated on the basis of gold-standard Fourier shell correlation of independently refined half maps and the 0.143 cutoff criterion. Local resolution was estimated in cryoSPARC using default parameters.

Model building and refinement

Predicted model of active-state SUCR1 receptor from Alphafold were used as initial model for rebuilding and refinement against the electron microscopy density map. UCSF Chimera-1.14[2] was used to dock the model into the electron microscopy density map, and followed by iterative manual adjustment and rebuilding in COOT-0.9.6[3] and ISOLDE-1.2[4]. Then models were further refined and validated in Phenix-1.20[5] programs (Table S1). Structural figures were generated using UCSF Chimera-1.14, ChimeraX-1.2[6] and PyMOL-2.0 (https://pymol.org/2/).

GloSensor cAMP assay

The GloSensor cAMP assay (Promega) was performed to monitor the real-time cAMP variation induced by SUCR1. In brief, the full-length SUCR1 were fused after HA signal peptide and Flag tag. The constructs were cloned into pcDNA3.0 vector for HEK293T system. Before transfection, HEK293T cells were plated onto 6-well plate with density of 1.5×10^5 cells/mL. After 16 hours, cells were transfected with 1.5 μg receptor and 1.0 μg GloSensor-22F (Promega). After 24 hours, transfected cells were digested and transferred onto 96-well plate with 50 μL suspension with density of 3×10^5 cells/ml. After another 16 hours, cells were starved by 50 μL Hank's balanced salt solution for 30 min and then incubated in 50 μL CO_2-independent media containing 2% GloSensor cAMP Reagent (Promega) for 1 hour. After incubation, 5.5 μL test ligands with various concentrations were added and incubated for 10 min at room temperature. For Gi-coupled SUCR1, additional 5.5 μL Forskolin were added to the cells in the final concentration of 1 μM. All luminescence signals are tested by EnVision multi-plate reader according to the manufacturer's instructions. All data were analyzed using Prism 9 (GraphPad) and presented as means ± S.E.M. from at least three independent experiments in technical duplicates or triplicates. Non-linear curve fit was performed using a three-parameter logistic equation [log (agonist vs response)]. The final curves were shown as normalization form compared to the wild-type. The significance was determined with two-side, one-way ANOVA followed by Fisher's LSD test compared with WT. *P<0.05; **P<0.01 and ***P<0.001 were considered as statistically significant.

REFERENCES

1 Liu, P. *et al.* The structural basis of the dominant negative phenotype of the Gαi1β1γ2 G203A/A326S heterotrimer. *Acta Pharmacol Sin* **37**, 1259-1272, doi:10.1038/aps.2016.69 (2016).

2 Pettersen, E. F. *et al.* UCSF Chimera--a visualization system for exploratory research and analysis. *J Comput Chem* **25**, 1605-1612, doi:10.1002/jcc.20084 (2004).

3 Emsley, P. & Cowtan, K. Coot: model-building tools for molecular graphics. *Acta Crystallogr D Biol Crystallogr* **60**, 2126-2132, doi:10.1107/s0907444904019158 (2004).

4 Croll, T. I. ISOLDE: a physically realistic environment for model building into low-resolution electron-density maps. *Acta Crystallogr D Struct Biol* **74**, 519-530, doi:10.1107/s2059798318002425 (2018).

5 Adams, P. D. *et al.* Recent developments in the PHENIX software for automated crystallographic structure determination. *J Synchrotron Radiat* **11**, 53-55, doi:10.1107/s0909049503024130 (2004).

6 Pettersen, E. F. *et al.* UCSF ChimeraX: Structure visualization for researchers, educators, and developers. *Protein Sci* **30**, 70-82, doi:10.1002/pro.3943 (2021).

Figure S1

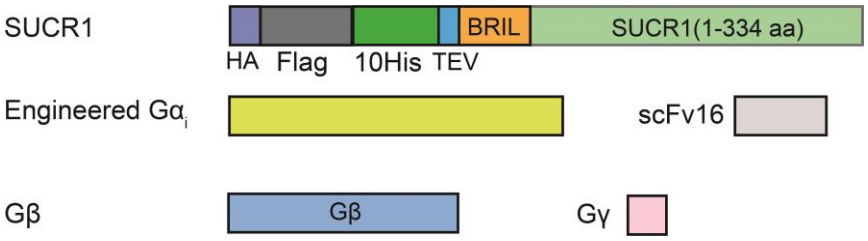

Figure S1. Cartoon models of the constructs used in this study.

Figure S2

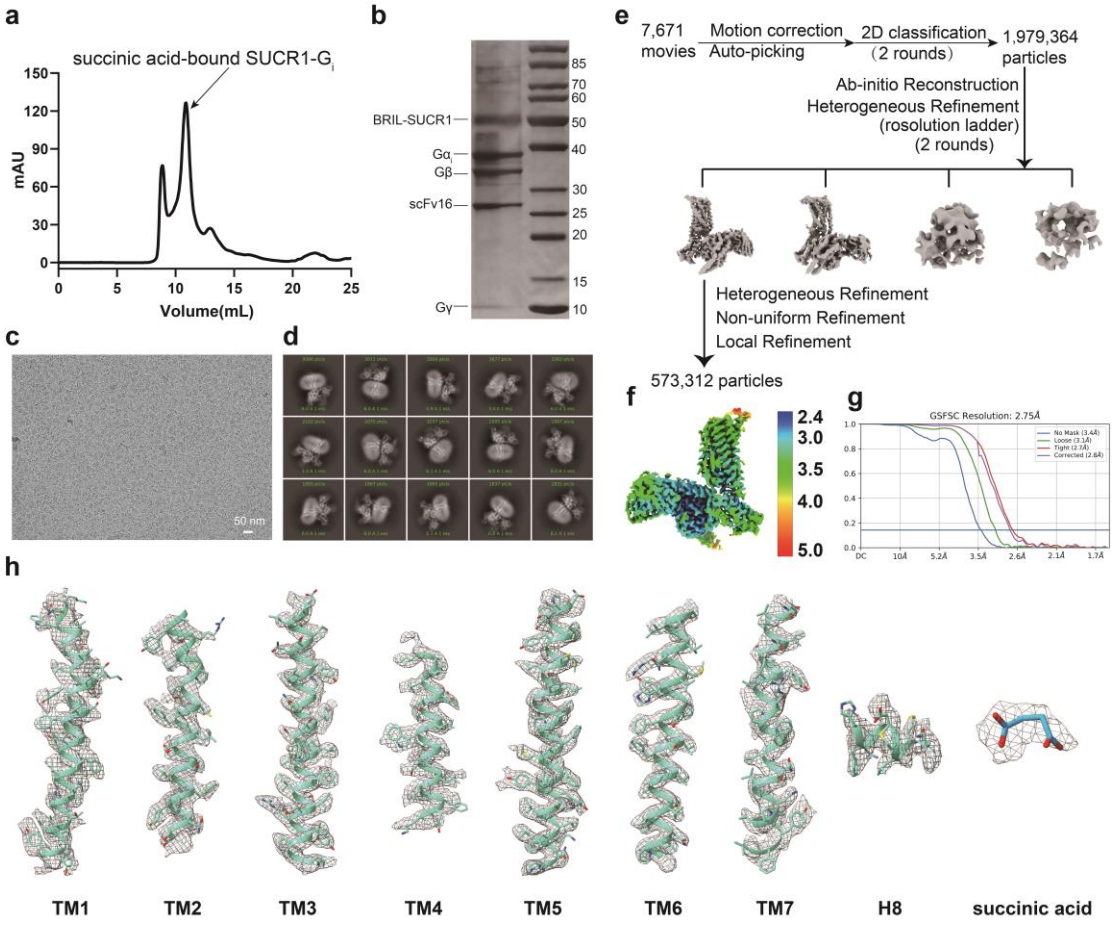

Figure S2. Structure determination of succinic acid-SUCR1-G_i complex.

a, b Size exclusion chromatography (SEC) profiles (**a**) and SDS-PAGE analysis (**b**) of SUCR1-G_i complex activated by succinic acid.

c, d Representative cryo-EM image (**c**) and 2D classification averages (**d**) of succinic acid-SUCR1-G_i.

e Cryo-EM data processing flowcharts of succinic acid - SUCR1-G_i.

f The global density map of succinic acid-SUCR1-G_i colored by local resolutions.

g The Fourier shell correlation (FSC) curves of succinic acid-SUCR1-G_i. The global resolution of the final processed density map estimated at the FSC = 0.143 is 2.75 Å.

h The density maps of helices TM1-TM7 of transmembrane domain, and

succinic acid in succinic acid-SUCR1-G_i.

Figure S3.

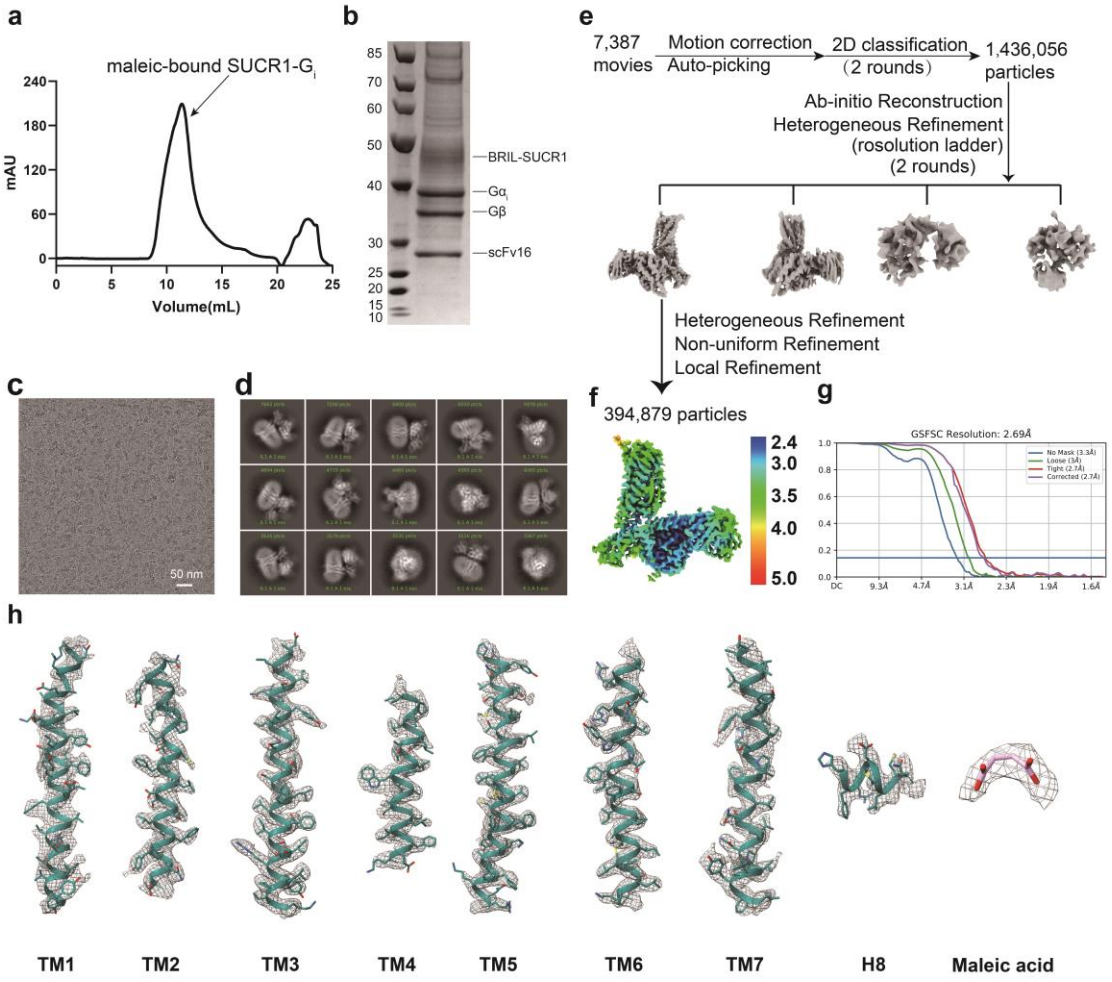

Figure S3. Structure determination of maleic acid-SUCR1-G_i complex.

a, b Size exclusion chromatography (SEC) profiles (**a**) and SDS-PAGE analysis (**b**) of SUCR1-G_i complex activated by maleic acid.

c, d Representative cryo-EM image (**c**) and 2D classification averages (**d**) of maleic acid-SUCR1-G_i.

e Cryo-EM data processing flowcharts of maleic acid-SUCR1-G_i.

f The global density map of maleic acid-SUCR1-G_i colored by local resolutions.

g The Fourier shell correlation (FSC) curves of maleic acid-SUCR1-G_i. The global resolution of the final processed density map estimated at the FSC = 0.143 is 2.68 Å.

h The density maps of helices TM1-TM7 of transmembrane domain, and maleic

acid in maleic acid-SUCR1-G_i.

Figure S4.

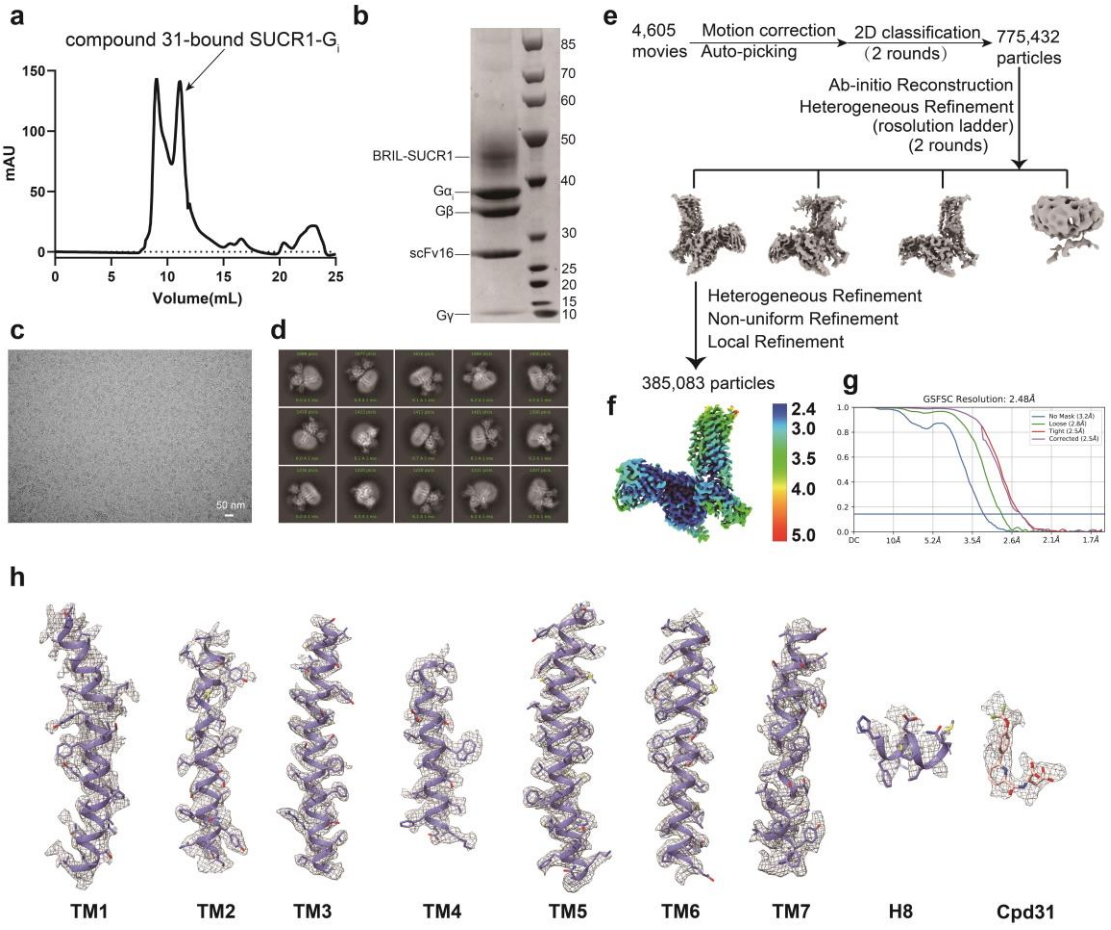

Figure S4. Structure determination of compound 31-SUCR1-G_i complex.

a, b Size exclusion chromatography (SEC) profiles (**a**) and SDS-PAGE analysis (**b**) of SUCR1-G_i complex activated by compound 31.

c, d Representative cryo-EM image (**c**) and 2D classification averages (**d**) of compound 31-SUCR1-G_i.

e Cryo-EM data processing flowcharts of compound 31 - SUCR1-G_i.

f The global density map of compound 31-SUCR1-G_i colored by local resolutions.

g The Fourier shell correlation (FSC) curves of compound 31-SUCR1-G_i. The global resolution of the final processed density map estimated at the FSC = 0.143 is 2.68 Å.

h The density maps of helices TM1-TM7 of transmembrane domain, and compound 31 in compound 31-SUCR1-G_i.

Figure S5.

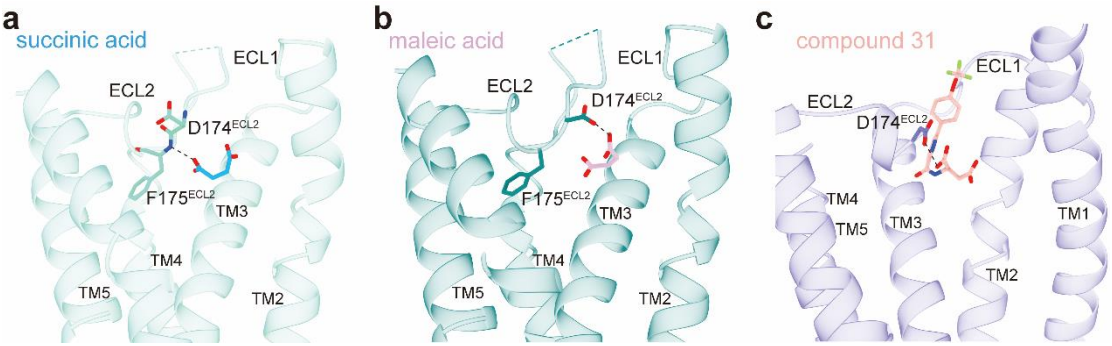

Figure S5. The interaction of D174^{ECL2} and succinic acid (a), maleic acid (b), and compound 31(c) in SUCR1 structures.

Figure S6.

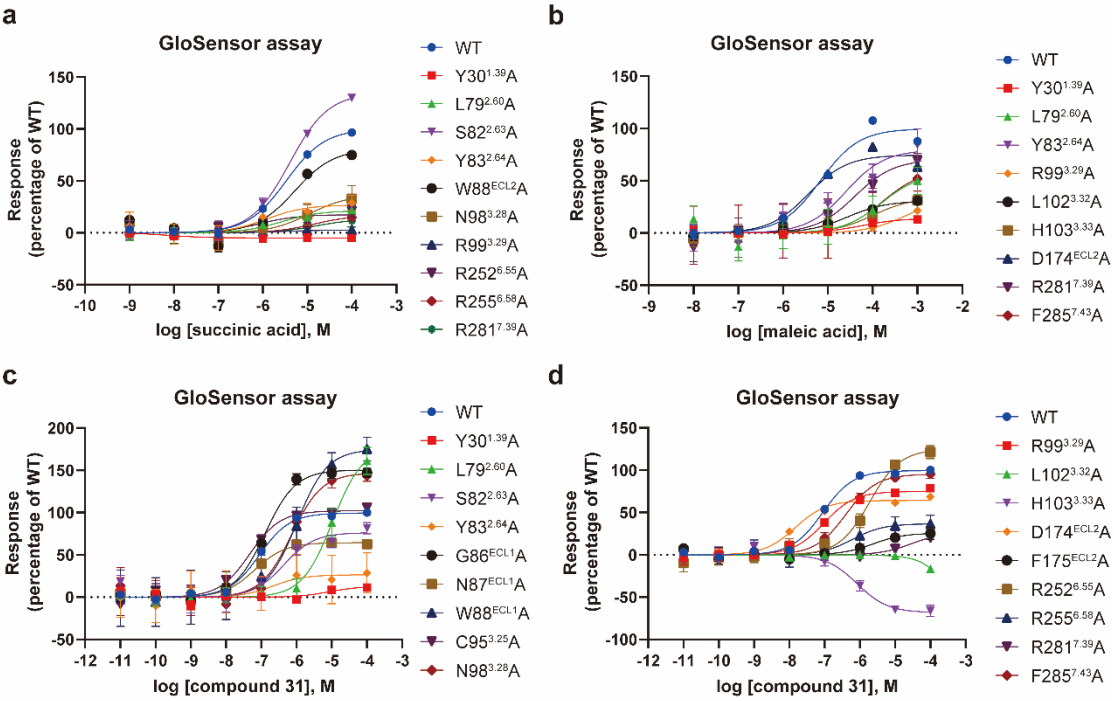

Figure S6. Evaluation of the mutational effects of SUCR1 induced by three agonists measured by GloSensor assay.

Concentration-response curves of wild-type/mutants of SUCR1 induced by the three agonists, succinic acid (**a**), maleic acid (**b**), and compound 31 (**c**). Every response of mutant was normalized to corresponding wild-type as 100%. Data are shown as means ± S.E.M. from a minimum of three independent experiments performed in technical duplicates.

Figure S7.

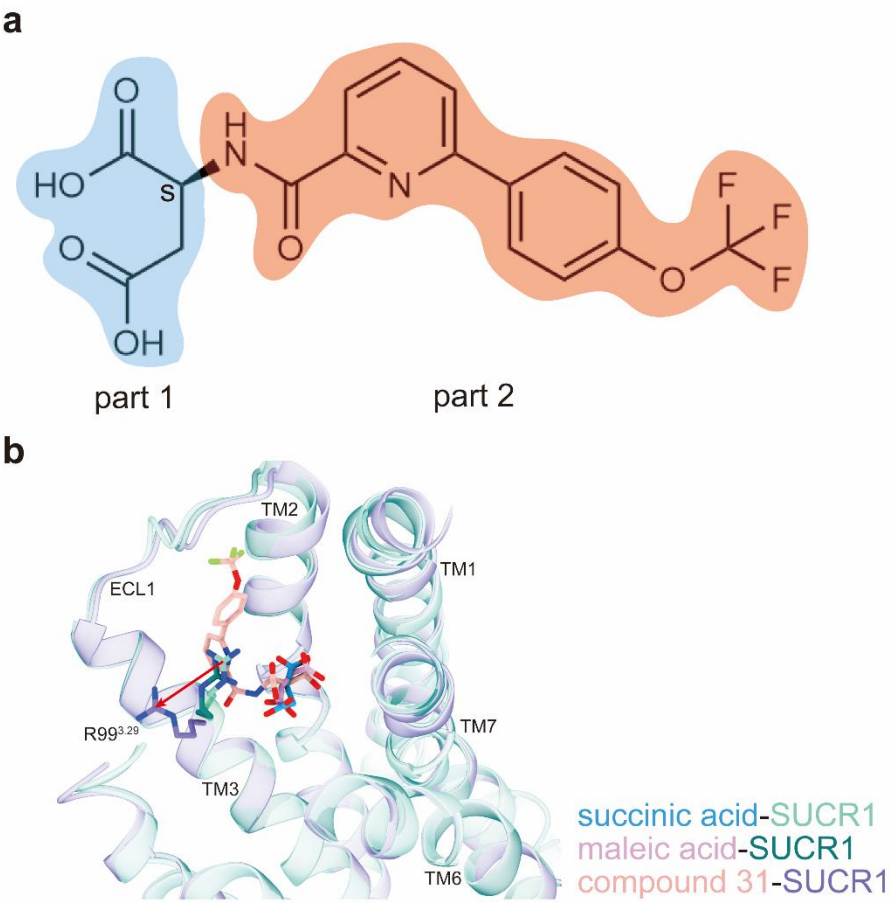

Figure S7. Chemical formula of compound 31 and Structural alignment of SUCR1 structures.

a Chemical formula of compound 31.

b Structural alignment indicated the movement of R99$^{3.29}$ during compound 31 insertion.

Table S1: Cryo-EM data collection, refinement and validation statistics

	SUCR1-G_i complex		
	succinic acid	**maleic acid**	**compound 31**
Voltage (kV)	300	300	300
Electron exposure ($e^-/Å^2$)	50	50	50
Defocus range (μm)	-1.0 to -2.0	-1.0 to -2.0	-1.0 to -2.0
Pixel size (Å)	0.824	0.73	0.824
Symmetry imposed	C1	C1	C1
Filtered particle images (no.)	1,979,364	1,436,056	775,432
Final particle images (no.)	573,312	394,879	385,083
Map resolution (Å)	2.75	2.69	2.48
FSC threshold	0.143	0.143	0.143
Map resolution range (Å)	2.4 - 5.0	2.4 - 5.0	2.4 - 5.0
Refinement			
Initial model used (PDB code)	AlphaFold SUCR1	AlphaFold SUCR1	AlphaFold SUCR1
Map sharpening *B* factor ($Å^2$)	-122.5	-110.6	-93.1
Model composition			
Non-hydrogen atoms	8,816	8,775	8,712
Protein residues	1,124	1,122	1,111
Ligands	1	1	1
B factors ($Å^2$)			
Protein	70.67	98.05	70.48
Ligand	117.68	20.00	20.00
R.m.s. deviations			
Bond lengths (Å)	0.004	0.005	0.004
Bond angles (°)	0.973	0.989	0.985
Validation			
MolProbity score	1.27	1.38	1.04
Clashscore	3.60	4.35	2.54
Poor rotamers (%)	0.00	0.00	0.00
Ramachandran plot			
Favored (%)	97.36	97.09	98.16
Allowed (%)	2.64	2.91	1.84
Disallowed (%)	0.00	0.00	0.00

Table S2. Potency of succinic acid activating WT and mutated SUCR1. The wild type (WT) and mutants of SUCR1 discussed in this manuscript were individually analyzed. The affinities are derived from at least 3 independent experiments using GloSensor function assay. The expression level of mutant SUCR1 were normalized to wild-type SUCR1 as 100%, respectively. Each data point represents mean ±standard error of the mean (S.E.M.). All data were analyzed by two-sided Student's t test. *P<0.05, **P<0.01, ***P<0.001 vs. WT. Source data are available online. Definitions: NA – not applicable; NT, not tested.

WT and mutants	Succinic acid induced Gi inhibition (pEC_{50} ± S.E.M)	Span (WT%) ± S.E.M
WT	5.48±0.02	100
Y30A	NA	NA
L79A	5.62±0.20	21.41±4.08**
S82A	5.40±0.06	134.7±5.25
Y83A	5.61±0.52	29.31±5.97**
W88A	5.29±0.04	80.60±1.88
N98A	6.17±1.17	28.32±33.32**
R99A	NA	NA
R252A	NA	NA
R255A	NA	NA
R281A	NA	NA

Table S3. Potency of maleic acid activating WT and mutated SUCR1. The wild type (WT) and mutants of SUCR1 discussed in this manuscript were individually analyzed. The affinities are derived from at least 3 independent experiments using GloSensor function assay. The expression level of mutant SUCR1 were normalized to wild-type SUCR1 as 100%, respectively. Each data point represents mean ±standard error of the mean (S.E.M.). All data were analyzed by two-sided Student's t test. *P<0.05, **P<0.01, ***P<0.001 vs. WT. Source data are available online. Definitions: NA – not applicable; NT, not tested.

WT and mutants	Maleic acid induced Gi inhibition (pEC_{50} ± S.E.M)	Span (WT%) ± S.E.M
WT	5.17±0.08	100
Y30A	NA	NA
L79A	3.78±0.06	58.06±5.45***
Y83A	4.63±0.07	79.56±16.37
R99A	3.20±0.21	37.54±4.86****
H103A	3.83±0.35	38.88±4.82**
D174A	5.44±0.04	74.55±5.63
R281A	4.57±0.37	70.66±13.94
F285A	3.92±0.22	61.06±37.02**

Table S4. Potency of compound 31 activating WT and mutated SUCR1. The wild type (WT) and mutants of SUCR1 discussed in this manuscript were individually analyzed. The affinities are derived from at least 3 independent experiments using GloSensor function assay. The expression level of mutant SUCR1 were normalized to wild-type SUCR1 as 100%, respectively. Each data point represents mean ± standard error of the mean (S.E.M.). All data were analyzed by two-sided Student's t test. *P<0.05, **P<0.01, ***P<0.001 vs. WT. Source data are available online. Definitions: NA – not applicable; NT, not tested.

WT and mutants	Compound 31 induced Gi inhibition (pEC_{50} ± S.E.M)	Span (WT%) ± S.E.M
WT	7.05±0.07	100
Y30A	NA	NA
L79A	4.95±0.13****	180.13±17.29**
S82A	6.38±0.12**	76.57±6.03
Y83A	NA	NA
G86A	6.88±0.12	150.9±14.14
N87A	7.17±0.05	64.53±4.80
W88A	5.98±0.04****	174.7±35.33**
C95A	7.32±0.16	102.88±20.52
N98A	6.08±0.16****	147.62±39.41
R99A	7.03±0.05****	74.90±8.81
L102A	NA	NA
H103A	6.15±0.32***	-69.74±7.96****
D174A	7.82±0.11****	64.41±8.08
F175A	5.55±0.17****	26.46±6.66**
R252A	5.72±0.08****	124.80±15.78
R255A	6.18±0.10**	36.50±16.26*
R281A	NA	NA
F285A	6.40±0.02	95.27±4.39